

See discussions, stats, and author profiles for this publication at: <https://www.researchgate.net/publication/267744613>

Structural and Magnetic Diversity Based on Different Imidazolate Linkers in Cu(II)-Azido Coordination Compounds

ARTICLE in INORGANIC CHEMISTRY · OCTOBER 2014

Impact Factor: 4.76 · DOI: 10.1021/ic501655u · Source: PubMed

CITATIONS

3

READS

41

6 AUTHORS, INCLUDING:



Anindita Chakraborty

Jawaharlal Nehru Centre for Advanced Scienti...

14 PUBLICATIONS 122 CITATIONS

[SEE PROFILE](#)



Srinivasa Rao Lingampalli

Jawaharlal Nehru Centre for Advanced Scienti...

14 PUBLICATIONS 85 CITATIONS

[SEE PROFILE](#)



Joan Ribas

375 PUBLICATIONS 11,939 CITATIONS

[SEE PROFILE](#)



Tapas Maji

Jawaharlal Nehru Centre for Advanced Scienti...

176 PUBLICATIONS 4,299 CITATIONS

[SEE PROFILE](#)

Structural and Magnetic Diversity Based on Different Imidazolate Linkers in Cu(II)-Azido Coordination Compounds

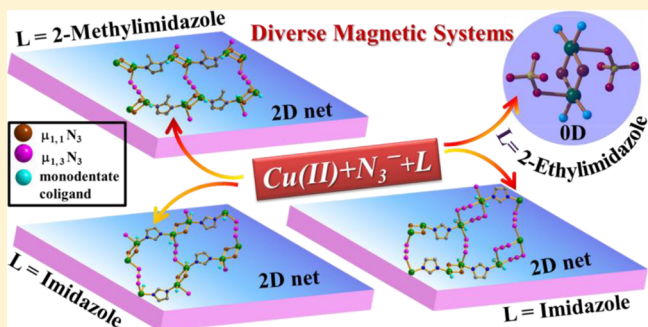
Anindita Chakraborty,[†] Srinivasa Rao Lingampalli,[†] Aman Kumari,[†] Joan Ribas,[‡] Jordi Ribas-Arino,[§] and Tapas Kumar Maji^{*,†}

[†]Molecular Materials Laboratory, Chemistry and Physics of Materials Unit, Jawaharlal Nehru Centre for Advanced Scientific Research, Jakkur, Bangalore 560 064, India

[‡]Departament de Química Inorgànica and [§]Departament de Química Física and IQTCUB, Universitat de Barcelona, Diagonal 645, 08028 Barcelona, Spain

Supporting Information

ABSTRACT: This Article reports the syntheses, structural characterization, and magnetic studies of four different Cu(II)-azido compounds based on imidazole or substituted imidazole ligand. The compounds, $[\text{Cu}_2(\mu_{1,1}\text{-N}_3)_2(\text{EtimiH})_4(\text{ClO}_4)_2]$ (**1**) (EtimiH = 2-ethylimidazole), $[\text{Cu}_2(\mu\text{-Meimi}^-)(\text{MeimiH})_2(\mu_{1,1}\text{-N}_3)_2(\mu_{1,3}\text{-N}_3)]_n$ (**2**) (MeimiH = 2-methylimidazole; $\mu\text{-Meimi}^-$ is the bridging mononegative anion of 2-methylimidazole), $[\text{Cu}_2(\mu\text{-imi}^-)(\text{imiH})_2(\mu_{1,1}\text{-N}_3)_2(\mu_{1,3}\text{-N}_3)]_n$ (**3**), and $[\{\text{Cu}_2(\mu_{1,1}\text{-N}_3)_2(\mu_{1,3}\text{-N}_3)(\mu\text{-imi}^-)(\text{imiH})_3\}\text{-H}_2\text{O}]_n$ (**4**) (imiH = imidazole; $\mu\text{-imi}^-$ = bridging mononegative anion of imidazole), have been synthesized by the self-assembly of Cu(II) salts, azide ion, and the corresponding imidazole bridging ligands. By changing the substitution on the second linker (imidazole or substituted imidazole) and varying synthetic conditions, diverse structural and magnetic features have been achieved in compounds **1–4**. Compound **1** has a double end-on azido bridged dinuclear core, while the other compounds (**2–4**) have 2D networks. Compound **2** and **3** contain 1D chains with alternate $\mu_{1,1}\text{-N}_3$ and $\mu\text{-Meimi}^-$ bridging, and such chains are further connected through a $\mu_{1,3}\text{-N}_3$ bridge to result in the formation of the 2D network. Compound **4** is a novel 2D coordination polymer consisting of a zigzag 1D coordination chain having $(\mu_{1,1}\text{-N}_3)_2$, $\mu\text{-imi}^-$, and $(\mu_{1,3}\text{-N}_3)_2$ bridging groups and the chains undergo bridging through a $\mu_{1,3}\text{-N}_3$ group resulting in the 2D network. Temperature dependent magnetic measurements show diverse magnetic properties of **1–4**. Such versatile magnetic behaviors have been correlated to the respective bridging mode of azide and the corresponding imidazole bridging ligands.



INTRODUCTION

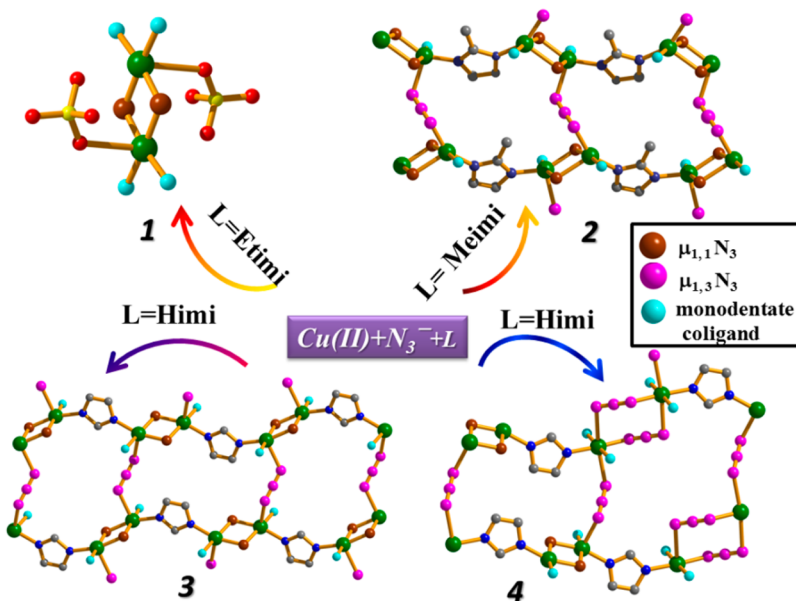
Coordination polymers or metal–organic hybrid materials have attracted significant research interest over the past few decades as a new class of molecular materials with several promising applications.¹ Intensive research over the past two decades has culminated in better understanding of the fundamental material properties of these structurally diverse compounds. Among these different properties, such as adsorption, luminescence, and magnetism, magnetism remains as a subject which still requires detailed investigations to understand the elementary magnetic behaviors.² Especially polynuclear clusters and extended networks of coordination polymers containing paramagnetic metal ions have attracted extensive research interest.³ Suitable bridging ligands mediate the magnetic exchange in these materials, and different factors such as appropriate bridging modes, strict and accidental orthogonality of the magnetic orbitals,⁴ spin polarization,⁵ and delocalization of unpaired electrons⁵ influence the type and magnitude of magnetic coupling between the paramagnetic centers. Azide is one of the well-explored bridging ligands for making efficient

molecular bridges to furnish such molecular magnets.⁶ The reason behind the excitement about the research on azide-based molecular magnets is due to azide's excellent ability to propagate different kinds of magnetic interactions, based on the different binding modes.⁶ The Cu-azido system demands special attention as a handful of novel structures can be designed owing to the flexible coordination geometry of Cu(II) with the different binding modes of azide.^{3b,6–8} Our group has been working on such problems with the motivation of understanding of the underlying magnetic behavior and proper structure–property relationship.^{3f–i} Following our work in this field, in this Article we present the structural and magnetic study of imidazole and substituted imidazole based Cu-azido systems. The reason behind the employment of imidazole or similar substituted imidazole ligands as a second linker in the Cu-azido system is threefold. First, the imidazolate (imi^-) ion, which is the deprotonated form of imidazole (imiH), is an

Received: July 11, 2014

Published: October 31, 2014

Scheme 1. Formation of Versatile Cu-Azido Coordination Compounds and the Different Binding Modes of the Bridging Ligands^a



^aThe monodentate coligands are EtimiH for **1**, MeimiH for **2** and imiH for **3** and **4** respectively. Color code: Cu, green; C, gray; N, blue; Cl, yellow; O, red.

efficient heterocyclic bridging ligand which provides a three-atom magnetic pathway between the paramagnetic metal centers.^{9a–d} Being able to provide a stronger three-atom bridge, the magnetic interaction would be much stronger than many other longer bridging ligands such as 4,4'-bipyridine,^{7a} pyrazine,^{7b} and different amines.⁶ Second, it can be used as a coligand with the azido ion to obtain new structural topology. Third, it would be interesting to study the effect of substitution (e.g., $-\text{CH}_3$, $-\text{CH}_2\text{CH}_3$, etc.) on the imidazole ring in a series of resulting structures and the corresponding changes in the magnetic behavior with the structural changes. Thus, bridging Cu(II) ions by these two different ligands (imidazole and azide) would provide interesting magnetic systems with versatile superexchange mechanisms. To the best of our knowledge, studies on metal–azide–imidazolate coordination polymers and their magnetic studies are limited and yet to be properly accounted for. We have strived to furnish such novel molecular systems and study the diversity in their structures and magnetism with the variation of the coligand (imidazole or substituted imidazole) and their stoichiometry. Herein we report the synthesis, structural characterization, and detailed magnetic properties of four new coordination compounds (see Scheme 1): $[\text{Cu}_2(\mu_{1,1}\text{-N}_3)_2(\text{EtimiH})_4(\text{ClO}_4)_2]$ (**1**) (EtimiH = 2-ethylimidazole), $[\text{Cu}_2(\mu\text{-Meimi}^-)(\text{MeimiH})_2(\mu_{1,1}\text{-N}_3)_2(\mu_{1,3}\text{-N}_3)]_n$ (**2**) (MeimiH = 2-methylimidazole; $\mu\text{-Meimi}^-$ = bridging mononegative anion of 2-methylimidazole), $[\text{Cu}_2(\mu\text{-imi}^-)\text{-}(\text{imiH})_2(\mu_{1,1}\text{-N}_3)_2(\mu_{1,3}\text{-N}_3)]_n$ (**3**), and $[\{\text{Cu}_2(\mu_{1,1}\text{-N}_3)_2(\mu_{1,3}\text{-N}_3)(\mu\text{-imi}^-)(\text{imiH})_3\}\cdot\text{H}_2\text{O}]_n$ (**4**) (imiH = imidazole; $\mu\text{-imi}^-$ = bridging mononegative anion of imidazole). It should be noted that judicious choice of the ligands and variation in the molar ratio of different starting compounds steered diverse binding modes and interesting structural features in **1–4**.

EXPERIMENTAL SECTION

Materials. All the reagents and solvents employed are commercially available and were used as supplied without further

purification. $[\text{Cu}_2(\text{OAc})_4\cdot(\text{H}_2\text{O})_2]$, $\text{Cu}(\text{ClO}_4)_2\cdot 6\text{H}_2\text{O}$, NaN_3 , imidazole, 2-methylimidazole, and 2-ethylimidazole were obtained from the Aldrich Chemical Co.

Synthesis. $[\text{Cu}_2(\mu_{1,1}\text{-N}_3)_2(\text{EtimiH})_4(\text{ClO}_4)_2]$ (**1**). $\text{Cu}(\text{ClO}_4)_2\cdot 6\text{H}_2\text{O}$ (0.5 mmol, 0.185 g) was dissolved in 10 mL of water. A 1 mmol (0.048 g) sample of 2-ethylimidazole was dissolved in 5 mL of methanol and was dropwise added to the above metal solution. The resulting blue colored solution was stirred for 10 min. Then an aqueous solution (5 mL) of NaN_3 (0.5 mmol, 0.0325 g) was dropwise added to the above reaction mixture. The resulting green colored solution was stirred for 1 h and filtered. The filtrate was kept for slow evaporation at room temperature, and after 1 week green crystals were isolated. Yield: 62%, relative to Cu. Selected IR data (KBr, cm^{-1}): 3355 br, 3155 m, 3137 m, 2976 m, 2938 m, 2090 s, 1563 m, 1462 m, 1322 m, 1080 s, 780 m, 713m, 622 m (Figure S1 in the Supporting Information). Anal. Calcd for $\text{C}_{20}\text{H}_{32}\text{Cu}_2\text{N}_4\text{O}_8\text{Cl}_2$: C, 30.23; H, 4.06; N, 24.68. Found: C, 30.18; H, 4.12; N, 25.18%. The phase purity was checked by comparing the powder X-ray diffraction (PXRD) pattern of the bulk powder sample with the simulated data from single crystal (Figure S2 in the Supporting Information).

$[\text{Cu}_2(\mu\text{-Meimi}^-)(\text{MeimiH})_2(\mu_{1,1}\text{-N}_3)_2(\mu_{1,3}\text{-N}_3)]_n$ (**2**). An aqueous solution (10 mL) of $[\text{Cu}_2(\text{OAc})_4\cdot(\text{H}_2\text{O})_2]$ (0.25 mmol, 0.099 g) was stirred with a methanolic solution (10 mL) of 2-methylimidazole (0.75 mmol, 0.0615 g) to mix well. To this resulting blue solution, aqueous solution (5 mL) of NaN_3 (0.75 mmol, 0.0487 g) was dropwise added to result in a green colored turbid solution. The resulting solution was stirred for 1 h and filtered. The filtrate was kept for slow evaporation at room temperature, and after 2 weeks block-shaped green crystals were isolated. Yield: 51%, relative to Cu. Selected IR data (KBr, cm^{-1}): 3438 br, 2976 m, 2060 s, 1616 m, 1571 m, 1408 m, 1310 m, 1275 m, 1153 m, 762 s, 665 m, 426 m (Figure S1 in the Supporting Information). Anal. Calcd for $\text{C}_{12}\text{H}_{15}\text{Cu}_2\text{N}_5$: C, 29.03; H, 3.05; N, 42.32. Found: C, 28.98; H, 3.12; N, 42.25%. The phase purity was confirmed from the good correspondence of the PXRD pattern of the bulk powder sample with the simulated data from single crystal (Figure S3 in the Supporting Information).

$[\text{Cu}_2(\mu\text{-imi}^-)(\text{imiH})_2(\mu_{1,1}\text{-N}_3)_2(\mu_{1,3}\text{-N}_3)]_n$ (**3**). A similar methodology as for **2** was adopted to synthesize compound **3** except that 2-methylimidazole was replaced by imidazole (0.75 mmol, 0.051 g). Green color block-shaped crystals of **3** were isolated after 15 days.

Yield: 69%, relative to Cu(II). Selected IR data (KBr, cm^{-1}): 3137 br, 2045 s, 1542 m, 1481 m, 1460 m, 1433 m, 1330 m, 1280 s, 1257 m, 1070 s, 950 m, 855 m, 770 m, 658 m (Figure S1 in the Supporting Information). Anal. Calcd for $\text{C}_9\text{H}_{11}\text{Cu}_2\text{N}_{15}$: C, 29.69; H, 2.43; N, 46.04. Found: C, 24.57; H, 2.38; N, 46.68%. The phase purity was checked by comparing the PXRD pattern of the bulk powder sample with the simulated data from single crystal (Figure S4 in the Supporting Information).

$[\{\text{Cu}_2(\mu_{1,1}-\text{N}_3)_2(\mu_{1,3}-\text{N}_3)(\mu-\text{imi}^-)(\text{imiH})_3\}\cdot\text{H}_2\text{O}]_n$ (**4**). $[\text{Cu}_2(\text{OAc})_4 \cdot (\text{H}_2\text{O})_2]$ (0.375 mmol, 0.149 g) was dissolved in 10 mL of water, 5 mL of methanol, and 5 mL of acetonitrile. Then 2 mmol of imidazole (0.136 g) was added to the metal solution, which resulted in a dark blue colored solution. After 5 min, 2 mmol (0.130 g) of sodium azide was added dropwise and the solution turned dark green. The resulting green solution was stirred for 1 h and filtered. The filtrate was kept for slow evaporation at room temperature, and after 7 days, dark green colored block-shaped crystals appeared. The crystals were isolated. Yield: 74%, relative to Cu(II). Selected IR data (KBr, cm^{-1}): 3130 br, 2949 m, 2045 s, 1541 m, 1491 m, 1322 m, 1135 m, 1064 s, 775 s, 652 s, 619 m (Figure S1 in the Supporting Information). Anal. Calcd for $\text{C}_{12}\text{H}_{17}\text{Cu}_2\text{N}_{17}$: C, 27.38; H, 3.26; N, 45.23. Found: C, 27.24; H, 3.15; N, 45.72%. The phase purity was checked by comparing the PXRD pattern of the bulk powder sample with the simulated data from single crystal (Figure S5 in the Supporting Information).

Caution! Although we have not experienced any problems with the compounds reported here, azido compounds of metal ions are potentially explosive in the presence of organic ligands and should be handled with care.

Single-Crystal X-ray Diffraction. X-ray single-crystal structural data of **1–4** were collected on a Bruker Smart-CCD diffractometer equipped with a normal focus, 2.4 kW sealed tube X-ray source with graphite monochromated Mo $\text{K}\alpha$ radiation ($\lambda = 0.710\,73\text{ \AA}$) operating at 50 kV and 30 mA. The program SAINT^{10a} was used for integration of diffraction profiles, and absorption correction was made with the SADABS^{10b} program. All the structures were solved by SIR 92^{10c} and refined by full matrix least-squares method using SHEXL-97.^{10d} All the non-hydrogen atoms were refined anisotropically and all the hydrogen atoms were fixed by HFIX and placed in ideal positions. All calculations were carried out using SHEXL 97, PLATON,^{10e} and WinGX system, version 1.70.01.^{10f} All crystallographic and structure refinement data of **1–4** are summarized in Table S1 in the Supporting Information.

Physical Measurements. Elemental analyses were carried out on a Thermo Fischer Flash 2000 elemental analyzer. IR spectra were recorded in KBr pellets on a Bruker IFS 66v/S spectrophotometer in the region 4000–400 cm^{-1} . Powder X-ray diffraction (PXRD) patterns were recorded on a Bruker D8 Discover instrument using Cu $\text{K}\alpha$ radiation. The magnetic measurements for polycrystalline powder samples of **1–4** were carried out using a vibrating sample magnetometer (VSM) in a physical property measurement system (PPMS; Quantum Design, USA). Susceptibility data were collected under an external applied magnetic field of 1000 Oe.

RESULTS AND DISCUSSION

Structural Description. $[\text{Cu}_2(\mu_{1,1}-\text{N}_3)_2(\text{EtimiH})_4(\text{ClO}_4)_2]$ (**1**). Single-crystal X-ray diffraction analysis reveals that complex **1** crystallizes in the monoclinic space group $P2_1/n$ and is a dinuclear complex with the molecular formula $[\text{Cu}_2(\mu_{1,1}-\text{N}_3)_2(\text{EtimiH})_4(\text{ClO}_4)_2]$ (Figure 1). Each of the Cu centers locates itself in a square pyramidal geometry and is coordinated to four nitrogen atoms and one oxygen atom. Two of the nitrogen atoms are from 2-ethylimidazole (N4, N6), and two are from azido ligands (coordinated through N1 and N1_a). One oxygen atom (O2) of the perchlorate anion occupies the apical position, while the remaining three perchlorate oxygens remain uncoordinated. Selected bond lengths and bond angles are given in Table 1. The equatorial bond lengths vary from 1.972(4) to 1.975(4) \AA , whereas the apical bond length is

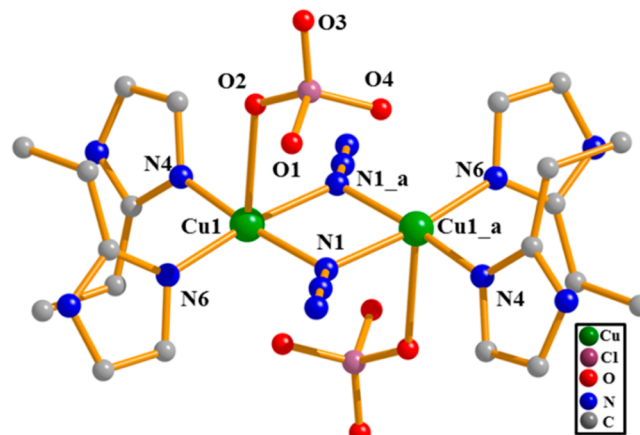


Figure 1. View of the dinuclear molecular complex **1**. Symmetry code: $a = 1 - x, 1 - y, 2 - z$.

2.639(5) \AA . The Cu1–N1–Cu1_a angle through the $\mu_{1,1}-\text{N}_3$ bridge is found to be 102.4(2) $^\circ$ in this complex. Cisoid angles are in the range from 77.6(2)–95.0(1) $^\circ$ and the transoid angles are 170.8(2) $^\circ$ and 171.2(1) $^\circ$, showing deviation from the ideal square pyramidal structure. The degree of distortion of the coordination polyhedron from square pyramid to trigonal bipyramidal can be calculated in terms of the Addison parameter (τ).¹¹ The Addison parameter, which has been calculated for Cu1, is 0.007, indicating that the geometry around Cu1 is very close to an ideal square pyramidal geometry. The pendant oxygen atom (O2) of the perchlorate anion forms a hydrogen bond with the –NH of the 2-ethylimidazole resulting in a two-dimensional (2D) supramolecular sheet in the crystallographic *bc* plane as shown in Figure S6 in the Supporting Information.

$[\text{Cu}_2(\mu-\text{Meimi}^-)(\text{MeimiH})_2(\mu_{1,1}-\text{N}_3)_2(\mu_{1,3}-\text{N}_3)]_n$ (**2**). Compound **2** crystallizes in the monoclinic space group $P2_1/c$ and the asymmetric unit consists of two crystallographically independent Cu(II) centers, both present in a distorted square pyramidal geometry. For Cu1, equatorial coordination sites are furnished by bridging μ -Meimi[–] ligand (N1), one monodentate pendant MeimiH (N3) ligand, bridging $\mu_{1,3}$ -azido (N7), and bridging $\mu_{1,1}$ -azido ligand (N10), whereas N13 of $\mu_{1,1}$ -azido ligand occupies the axial position. Cu2 adopts similar binding modes, where N2, N5, N10, N13, and N9 occupy the coordination sites, among which N9 is in the axial position (Figure 2a). Selected bond lengths and bond angles are given in Table 1. Equatorial Cu–N bond distances are in the range 1.964(2)–2.037(3) \AA , and distances in the axial positions are 2.290(2) and 2.362(3) \AA for Cu1 and Cu2, respectively. The Addison parameter values for Cu1 and Cu2 are 0.39 and 0.31 respectively, suggesting high distortion of the square pyramid around Cu1 and Cu2. Cisoid angles are in the range from 72.1(1) to 98.62(1) $^\circ$ and the transoid angles are in the range 148.8(1)–172.1(1) $^\circ$, showing deviation from the ideal square pyramidal structure. Cu1 and Cu2 are connected to each other via μ -Meimi[–] and asymmetric ($\mu_{1,1}-\text{N}_3$)₂ bridging alternatively resulting in the formation of a one-dimensional (1D) coordination polymer (Figure 2a). The angles Cu1–N13–Cu2 and Cu1–N10–Cu2 are 98.62(1) and 106.3(1) $^\circ$ respectively, and are important parameters for determining the type and strength of the magnetic exchange. In the 1D chain, distances between Cu1 and Cu2 through $\mu_{1,1}$ -azido and μ -Meimi[–] bridge are 3.251 and 5.965 \AA , respectively. Each chain further assembles via $\mu_{1,3}$ -azido bridging forming a 2D

Table 1. Selected Bond Lengths (\AA) and Angles (deg) for Compounds 1–4^a

Compound 1			
Cu1–N1	1.975(4)	Cu1–N4	1.972(4)
Cu1–N6	1.972(4)	Cu1–O2	2.639(5)
N1_a–Cu1–N4	93.7(2)	N1_a–Cu1–N6	171.2(1)
N1–Cu1–N1_a	77.6(2)	N4–Cu1–N6	95.0(1)
N1–Cu1–N4	170.8(2)	N1–Cu1–N6	93.8(2)
Cu1–N1–Cu1_a	102.4(2)		
Compound 2			
Cu1–N1	1.974(2)	Cu1–N3	1.976(2)
Cu1–N7	2.037(3)	Cu1–N10	2.028(2)
Cu1–N13	2.290(2)	Cu2–N2	1.964(2)
Cu2–N5	1.987(2)	Cu2–N13	1.990(3)
Cu2–N10	2.035(2)	Cu2–N9	2.362(3)
N1–Cu1–N3	94.8(1)	N1–Cu1–N7	148.8(1)
N1–Cu1–N10	87.4(1)	N3–Cu1–N7	92.0(1)
N3–Cu1–N10	72.1(1)	N7–Cu1–N10	90.10(1)
N2–Cu2–N5	96.32(1)	N2–Cu2–N13	96.1(1)
N2–Cu2–N10	149.3(1)	N5–Cu2–N13	67.62(1)
N5–Cu2–N10	88.6(1)	N10–Cu2–N13	81.0(1)
N3–Cu1–N10	172.1(1)	N5–Cu2–N13	167.62(1)
Cu1–N10–Cu2	106.3(1)	Cu1–N13–Cu2	98.62(1)
Compound 3			
Cu1–N1	2.016(7)	Cu1–N1_a	2.018(7)
Cu1–N4	2.371(8)	Cu1–N7	1.989(7)
Cu1–N9	1.976(6)	Cu2–N10	1.972(5)
Cu2–N11	1.985(6)	Cu2–N13	2.021(7)
Cu2–N6	2.380(8)	Cu2–N13_a	2.035(6)
N1–Cu1–N4	97.3(3)	N1–Cu1–N7	167.8(3)
N1–Cu1–N9	92.9(3)	N1–Cu1–N1_a	76.0(3)
N7–Cu1–N9	92.2(3)	N1_a–Cu1–N7	96.6(3)
N1_a–Cu1–N9	163.8(2)	N10–Cu2–N11	93.8(3)
N10–Cu2–N13	92.9(3)	N10–Cu2–N13_a	163.8(3)
N11–Cu2–N13_a	95.3(3)	N11–Cu2–N13	170.1(3)
N6–Cu2–N11	91.3(3)	Cu2–N13–Cu2_a	103.5(3)
Cu1–N1–Cu1_a	104.0(3)		
Compound 4			
Cu1–N1	1.969(3)	Cu1–N3	2.323(3)
Cu1–N6	1.983(3)	Cu1–N8_a	2.031(3)
Cu1–N8	2.027(3)	Cu2–N2	1.999(3)
Cu2–N11	1.995(3)	Cu2–N13	1.996(3)
Cu2–N15	2.019(3)	Cu2–N5	2.625(4)
Cu2–N17	2.664(4)		
N1–Cu1–N6	94.0(1)	N1–Cu1–N8_a	91.8(1)
N1–Cu1–N8	163.41(1)	Cu1–N3–N4	118.8(3)
N3–Cu1–N6	96.32(1)	N3–Cu1–N8	93.3(1)
N3–Cu1–N8_a	95.6(1)	N6–Cu1–N8_a	168.7(1)
N6–Cu1–N8	95.30(1)	N8–Cu1–N8_a	76.8(1)
Cu1–N8–Cu1_a	103.3(1)	N2–Cu2–N11	92.0(1)
N2–Cu2–N13	89.4(1)	N2–Cu2–N15	176.0(1)
N2–Cu2–N17_a	90.3(1)	N11–Cu2–N13	178.1(1)
N11–Cu2–N15	92.0(1)	N5–Cu2–N11	87.2(1)
N11–Cu2–N17	88.41(1)	N13–Cu2–N15	86.8(1)
N13–Cu2–N17	90.3(1)	N5–Cu2–N15	85.41(1)

^aSymmetry codes: for compound 1, $a = 1 - x, 1 - y, 2 - z$; for 3, $a = 1 - x, 1 - y, 1 - z$; for 4, $a = 2 - x, -1 - y, -z$.

network lying in the crystallographic bc plane, and the 2D net can be viewed as an assembly of repeating hexanuclear units (Figure 2b). Topological analysis of the 2D network using TOPOS 4.0^{10e} suggests a three-connected uninodal net and the

simplified 2D net is shown in Figure 3. In the 2D sheet, the distance between Cu1 and Cu2 through $\mu_{1,3}$ -azido bridging is 5.560 \AA .

$[\text{Cu}_2(\mu\text{-imi}^-)(\text{imiH})_2(\mu_{1,1}\text{-N}_3)_2(\mu_{1,3}\text{-N}_3)]_n$ (3). Compound 3 crystallizes in the triclinic space group $P\bar{1}$. Single-crystal X-ray diffraction analysis reveals that 3 is a 2D coordination polymer comprised of a 1D coordination chain with alternate imidazole and $\mu_{1,1}$ -azido bridging, similar to compound 2. In compound 3, there are two crystallographically independent Cu(II) centers in the asymmetric unit, both adopting distorted square pyramidal geometry (Figure 4). For Cu1, equatorial coordination sites are occupied by bridging $\mu\text{-imi}^-$ ligand (N9), one monodentate imiH (N7) ligand, and bridging $\mu_{1,1}$ -azido ligand (N1 and its symmetry related counterpart N1_a), whereas N4 of $\mu_{1,3}$ -azido ligand occupies the axial position. Similarly, Cu2 locates itself in a coordination environment similar to that of Cu1, where N10, N11, N13, and N13_a furnish the equatorial coordination sites while N6 is present at an axial position. Equatorial Cu–N bond distances are in the range 1.972(5)–2.035(6) \AA , and the axial bond distances are 2.371(8) and 2.380(8) \AA for Cu1 and Cu2, respectively. The Addison parameter values for Cu1 and Cu2 are 0.06 and 0.10, respectively. Cu1 and its symmetry related counterpart Cu1_a are connected to each other by the symmetrical $(\mu_{1,1}\text{-N}_3)_2$ bridging, through N1 and N1_a atoms. Similarly N13 and N13_a bind Cu2 and its symmetry related counterpart Cu2_a. The angles Cu1–N1–Cu1_a and Cu2–N13–Cu2_a are 104.0(3) and 103.5(3) $^\circ$, respectively. The bridging $\mu\text{-imi}^-$ creates a connection between Cu1 and Cu2. The structure can be described as a 1D chain of Cu1 and Cu2 held together by the bridging $\mu\text{-imi}^-$ and $\mu_{1,1}$ -azido ligand alternately (Figure 5). The 1D coordination chain further constructs a 2D network via $\mu_{1,3}$ -azido bridging through N4 and N6 atoms (Figure 5). The 2D net is composed of two different kinds of hexanuclear building units (Figure 5). In the 2D network, distances between the Cu1 and Cu2 through $\mu_{1,1}$ -azido and $\mu\text{-imi}^-$ bridge are 3.180 and 5.981 \AA respectively, while the distance through $\mu_{1,3}$ -azido is 6.183 \AA .

As we have previously discussed, both compounds 2 and 3 contain 1D chains with alternate $\mu\text{-imi}^-$ and $\mu_{1,1}$ -azido bridging and the 1D chains are further bridged through $\mu_{1,3}$ -azido bridging forming 2D networks. However, there are some distinct differences between the structural aspects of 2 and 3. First, the degree of distortion of the 5-coordinated Cu(II) centers are different. As is evident from the Addison parameters (0.39, 0.31 for 2; 0.06 and 0.10 for 3), the Cu(II) centers in 2 are more distorted from ideal square pyramidal geometry than those of 3. Furthermore, if we consider the hexanuclear building unit in the respective 2D net, 2 contains only one repeating unit while two different units are present in 3 (Figures 2b and 5).

The spatial orientations of the $\mu\text{-Meimi}^-$ or $\mu\text{-imi}^-$ bridging ligands in the corresponding 2D nets are also different (Scheme 1), which is expected to arise from the variation of the substitution on the imidazole ring. The $\mu\text{-Meimi}^-$ ligand in 2 tries to avoid steric hindrance because of the methyl group and thus cannot afford the formation of hexanuclear units which are observed in 3. Indeed, 2 adopts a more symmetric structure with only one kind of hexanuclear building unit and eventually crystallizes in the more symmetric monoclinic space group $P2_1/c$, while 3 with two different hexanuclear units crystallizes in the triclinic $P\bar{1}$ space group.

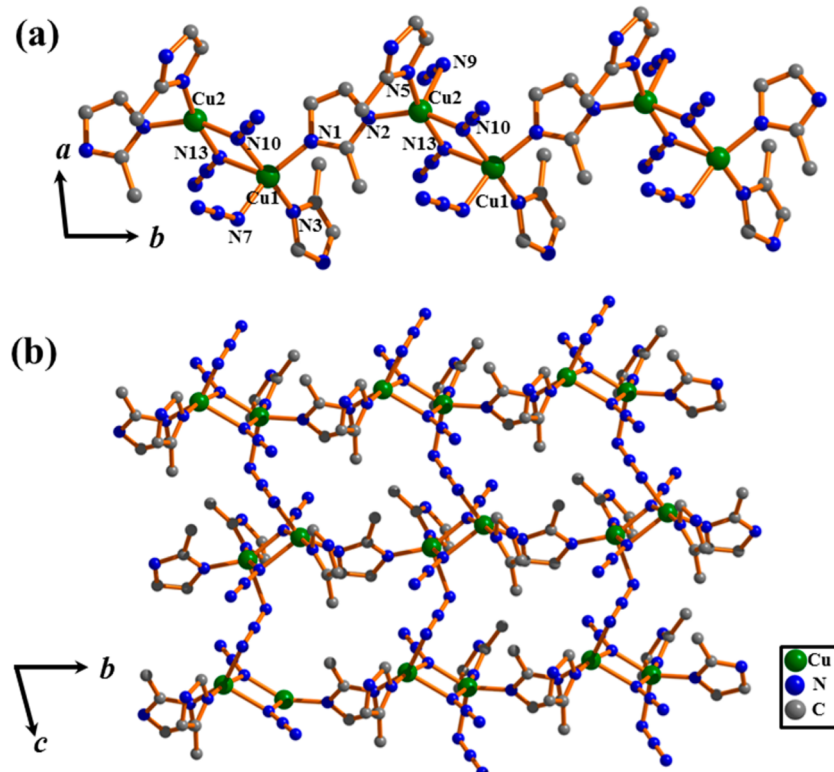


Figure 2. (a) View of the 1D alternate chain of compound 2. The coordination environments around each Cu(II) ion have also been shown. (b) View of the 2D network of compound 2 constructed by the $\mu_{1,3}$ -azido bridging between the 1D chains.

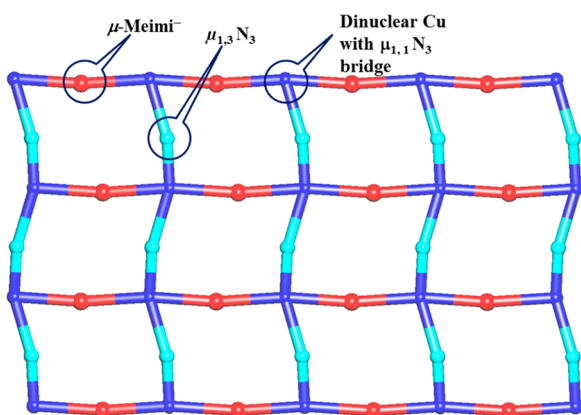


Figure 3. Simplified net of compound 2. The terminal monodentate ligands are not shown.

*[Cu₂($\mu_{1,1}$ -N₃)₂($\mu_{1,3}$ -N₃)(μ -imi⁻)(imiH)₃]·H₂O*_n (**4**). Compound 4 crystallizes in the triclinic $P\bar{1}$ space group and the structure determination by single-crystal X-ray diffraction reveals a 2D coordination polymer of Cu(II), the construction of which is facilitated by different bridging azide ligands along with a bridging imidazole ligand. In the asymmetric unit, there are two crystallographically independent Cu(II) centers (Cu1 and Cu2) having different coordination environments (Figure 6). Cu1 is found in a distorted square pyramidal geometry (4 + 1). For Cu1 the equatorial plane is occupied by four nitrogen atoms, N1 and N6 of two different imidazole ligands and N8 and N13 a nitrogen atoms of the two symmetry related bridging $\mu_{1,1}$ -N₃ ligands. The axial position is occupied by N3 nitrogen atom from the bridging azide $\mu_{1,3}$ -N₃ ligand. The degree of distortion from the ideal square pyramidal geometry is reflected in the angles of the equatorial plane of the Cu1 atom (Table 1). The equatorial Cu–N bond lengths are in the range 1.969(3)–

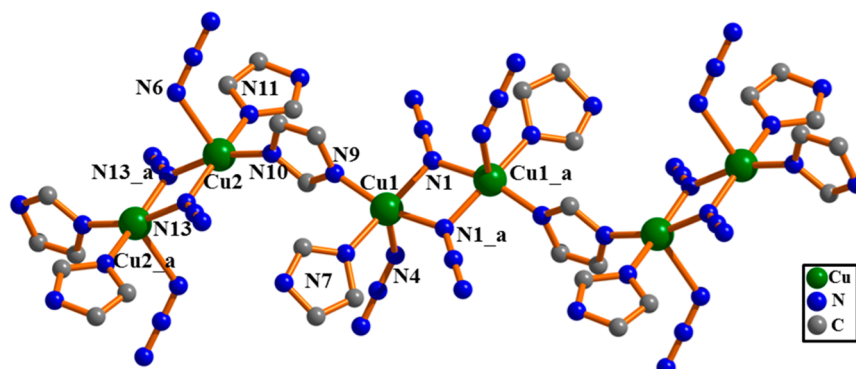


Figure 4. View of the coordination environment around each Cu^{II} ion of compound 3. Symmetry code: $a = 1 - x, 1 - y, 1 - z$.

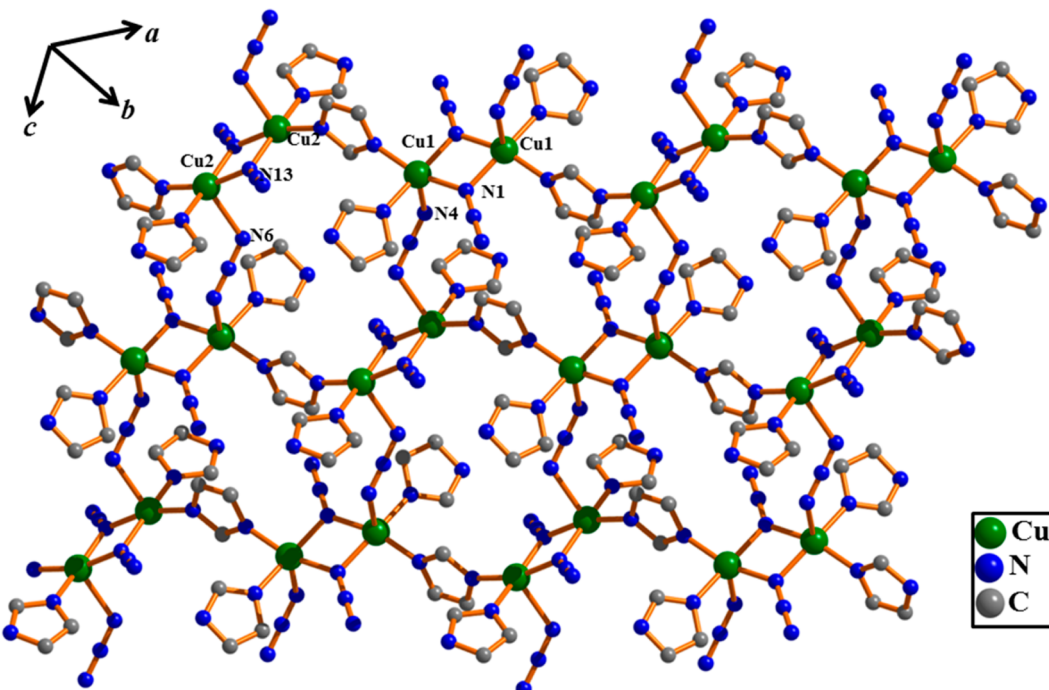


Figure 5. View of the 2D network of compound 3 constructed by the $\mu_{1,3}$ -azido bridging between the 1D chains.

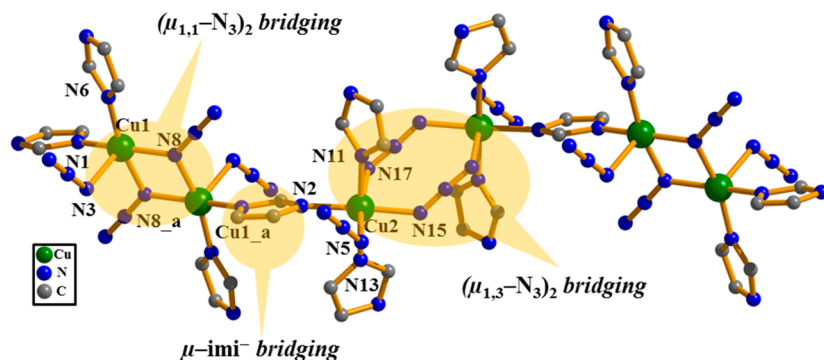


Figure 6. View of the coordination environment around each Cu^{II} ion of compound 4. The different bridging groups have been highlighted. Symmetry code: $a = 2 - x, -1 - y, -z$.

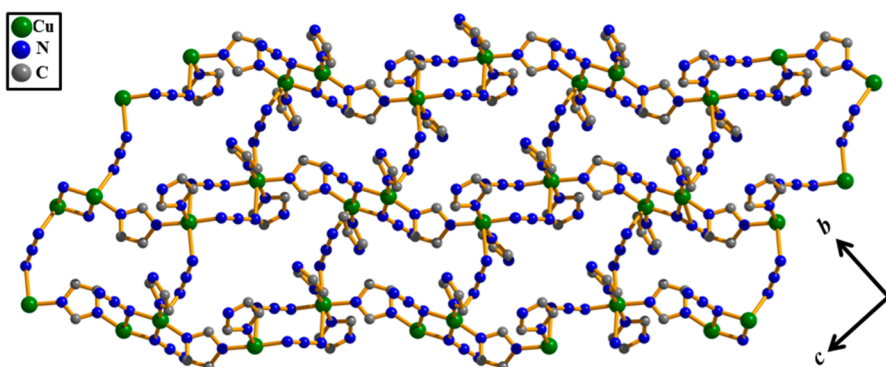


Figure 7. View of the 2D network of 4 lying in the crystallographic bc plane.

2.031(3) Å, while the axial Cu1–N3 distance is 2.323(3) Å. Cu2 is present in a distorted octahedral geometry (4 + 2), and the equatorial coordination sites are furnished by N2, N11, and N13 nitrogen atoms of the three imidazole ligands and N15 nitrogen atom of the bridging $\mu_{1,3}$ -N₃ ligand. The axial positions are occupied by N5 and N17 nitrogen atoms of two different

bridging $\mu_{1,3}$ -N₃ ligands. The equatorial Cu–N bond lengths are in the range 1.995(3)–2.019(3) Å, while the axial Cu–N bond lengths are 2.625(4) and 2.664(4) Å, respectively. The Cu(II) centers form a zigzag one-dimensional coordination chain, the formation of which is assisted by consecutive

bridging units having $(\mu_{1,1}\text{-N}_3)_2(\mu\text{-imi}^-)\text{-}(\mu_{1,3}\text{-N}_3)_2(\mu\text{-imi}^-)$ groups (Figures 6 and 8).

In the 1D coordination chain, Cu1 and its symmetry related counterpart are bridged via a symmetric $(\mu_{1,3}\text{-N}_3)_2$ group, while a symmetric $(\mu_{1,1}\text{-N}_3)_2$ group bridges Cu2 and its symmetry related counterpart Cu2_a. Finally, Cu1 and Cu2 are bridged by the $\mu\text{-imi}^-$ group. The distance between Cu1 and Cu1_a through the bridging $\mu_{1,1}\text{-N}_3$ ligand is 3.182 Å and the Cu1–N8–Cu1_a angle is found to be 103.25(2)°. The distance between Cu1 and Cu2 through the bridging $\mu\text{-imi}^-$ ligand is 5.976 Å. The 1D coordination chains are further connected to each other by the $\mu_{1,3}$ bridging azido group to furnish the 2D network along the crystallographic bc plane (Figure 7). The simplified 2D net is shown in Figure 8. The $\mu_{1,3}$ azido group bridges Cu1 of one chain and Cu2 of another chain, and the distance between these Cu(II) centers through this $\mu_{1,3}\text{-N}_3$ bridging is 6.240 Å.

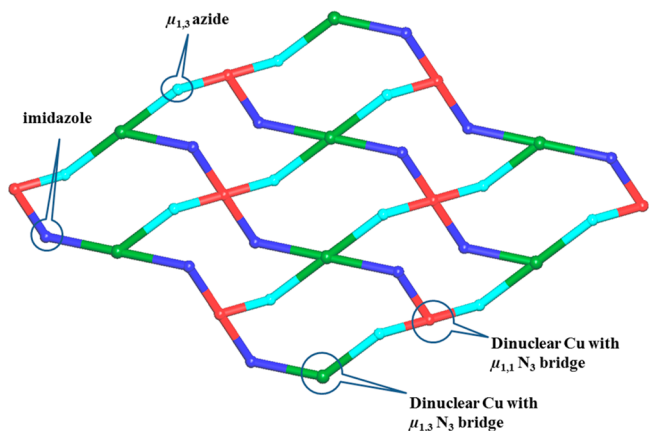


Figure 8. View of different bridging groups and the simplified net of compound 4. The terminal monodentate ligands are not shown.

Structural Correlations in 1–4. The formation of different Cu-azido compounds (**1–4**) with diverse binding modes from similar reagents is remarkable (Scheme 1). The distinct difference of compound **1** with respect to the other 2D compounds (**2–4**) in terms of dimensionality can be noted. The reason for the formation of a discrete dinuclear complex **1** is probably due to the larger steric effect of 2-ethylimidazole, which inhibits formation of a higher dimensional network. It is noteworthy that we have tried to synthesize different Cu-EtimiH-azide systems (other than **1**) by employing several reaction conditions (e.g., changing the EtimiH:azide concentration, varying solvent, etc.), but could not isolate any different single crystal, which suggests that **1** is probably the most stable structure without any steric crowding.

Yu and co-workers have reported a mononuclear Cu(II)-imidazole-azido compound with the formula $[\text{Cu}(\text{imiH})_4(\text{N}_3)_2]$, where pendant imidazole and monodentate azide ligands are present.^{9e} Our work shows that, by using such relatively smaller coligands (imiH and MeimiH), various azido binding modes and formation of 2D networks (in **2–4**; see Structural Description) can be observed. Under similar synthetic reaction conditions (stoichiometry Cu(II):MeimiH/imiH:azide = 0.5:0.75:0.75), use of MeimiH and imiH resulted in **2** and **3** respectively, which are structurally very similar. However, as we have discussed earlier, as a consequence of the difference in the substitution on the respective imidazole rings, they differ significantly in terms of the spatial orientation of the

bridging ligands and the respective 2D nets. By changing the stoichiometry (Cu(II):imiH:azide = 0.75:2:2) and employing imidazole as the coligand, we were able to furnish compound **4**, which consists of even more diverse binding modes of azido ligand than those of **2** and **3**. Thus, by varying the reaction condition slightly, higher dimensional networks having various structural motifs could be achieved with a smaller coligand such as imidazole. In our effort to furnish such higher dimensional networks, we synthesized another compound with the formula $[\text{Cu}_3(\text{imiH})_4(\mu\text{-imi}^-)_2(\text{N}_3)_4]_n$ (**5**) by the self-assembly of Cu(II) salt with imiH and azide at room temperature (stoichiometry Cu(II):MeimiH/imiH:azide = 0.75:1.5:1). Compound **5** is a 2D compound where linear 1D chains are present with alternating dinuclear units and mononuclear units. There are two different dinuclear units with the formulas $[\text{Cu}_2(\text{imiH})_2(\mu\text{-imi}^-)_2(\mu_{1,1}\text{-N}_3)_2(\mu_{1,3}\text{-N}_3)_2]^{2-}$ and $[\text{Cu}_2(\text{imiH})_2(\mu\text{-imi}^-)_2(\mu_{1,1}\text{-N}_3)_2(\text{N}_3)_2]^{2-}$ and a mononuclear unit with the formula $[\text{Cu}_2(\text{imiH})_2(\mu\text{-imi}^-)_2(\mu_{1,1}\text{-N}_3)]^-$. Interchain $\mu_{1,3}\text{-N}_3$ bridging between the mononuclear unit and the nearest neighboring dinuclear unit of the adjacent chain results in a 2D network (Figure S7 in the Supporting Information). Later a literature survey showed that this compound was reported by Nakamura et al.,^{9d} where they observed the ferrimagnetic behavior of the compound. We have also tried to isolate methylimidazole substituted compounds similar to **4** or **5**, but despite several attempts we could not obtain any structure other than **2**. We hypothesize that here the steric factor of 2-methylimidazole plays a role which probably inhibits formation of 2D nets similar to **4** or **5**. The formation of such different compounds by changing the reaction conditions such as stoichiometry and substitution on the coligand suggests that versatile 2D Cu-azido systems can indeed be fabricated with the aid of imidazole based ligands.

Magnetic Properties of Complex 1. The magnetic properties of complex **1** as a $\chi_M T$ vs T plot (χ_M is the molar magnetic susceptibility for two Cu^{II} ions) and the $M/N\beta$ vs H plot (magnetization M is expressed in $N\beta$ unit where N is the Avogadro number and β is the electronic Bohr magneton) are shown in Figure 9. Starting from room temperature, $\chi_M T$ values

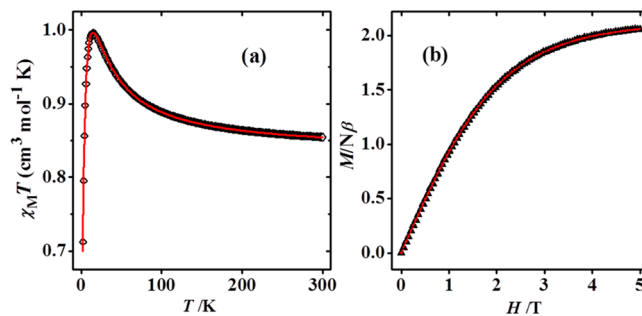


Figure 9. (a) Plot of $\chi_M T$ vs T for **1**. The solid red line indicates the best fit obtained (see text). (b) Plot of the reduced magnetization ($M/N\beta$) at 2 K. The solid red line indicates the best fit obtained (see text).

gradually increase up to 15 K (Figure 9a) and the $\chi_M T$ value at 15 K is close to $1.00 \text{ cm}^3 \text{ mol}^{-1} \text{ K}$. Below 15 K, the $\chi_M T$ values decrease quickly to $0.72 \text{ cm}^3 \text{ mol}^{-1} \text{ K}$ at 2 K. This feature is characteristic of an intramolecular ferromagnetic coupling with weak intermolecular antiferromagnetic interactions. Above 20 K, the $1/\chi_M$ vs T plot (Figure S8 in the Supporting Information) is well fitted by the Curie–Weiss law ($\chi_M = C/(T - \theta)$), with $C = 0.84 \text{ cm}^3 \text{ mol}^{-1} \text{ K}$ and $\theta = 4.9 \text{ K}$. The

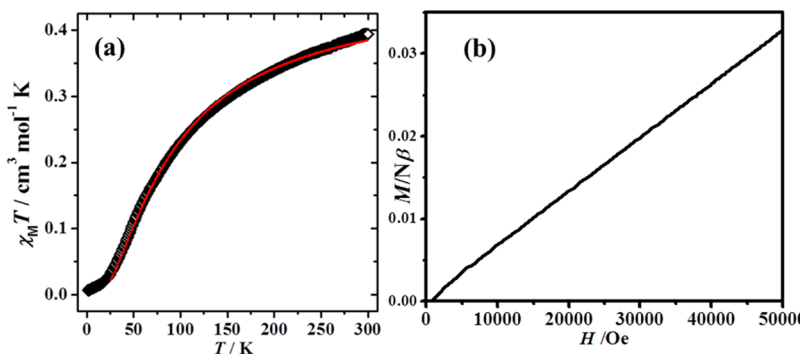


Figure 10. (a) Plot of $\chi_M T$ vs T for 2 per one Cu center. The solid red line indicates the best fit obtained (see text). (b) Plot of the reduced magnetization ($M/N\beta$) (per two Cu centers) at 2 K for compound 2.

positive Weiss constant indicates ferromagnetic interaction operates in 1. The reduced molar magnetization at 2 K is shown in Figure 9b. The saturation value at 5 T reaches a value close to $2.0N\beta$ (typical for two isolated or weakly coupled copper ions).

Complex 1 is a dinuclear compound with doubly $\mu_{1,1}\text{-N}_3$ bridging ligand, and the dinuclear entities are assembled through the supramolecular hydrogen bonding interaction (as discussed in the structural discussion). The fit of the susceptibility data has been carried out applying a modified Bleaney–Bowers formula, considering the mean field approach for taking into account the intermolecular interactions.^{3e} The best-fit parameters obtained are $J = +22.5(5)$ cm^{-1} , $z'J'(\text{intermolecular}) = -1.13(1)$ cm^{-1} , $g = 2.11(1)$, and $R = 1.0 \times 10^{-8}$ ($R = \sum_i [(\chi_M T)_{\text{obs}} - (\chi_M T)_{\text{calc}}]^2 / \sum_i [(\chi_M T)_{\text{obs}}]^2$). The fit of the magnetization data has been carried out by a full-diagonalization method using the MAGPACK program.¹⁵ The best-fit parameters obtained are $J = +23.2(3)$ cm^{-1} , $z'J'(\text{intermolecular}) = -1.21(2)$ cm^{-1} , $g = 2.12(1)$, and $R = 1.5 \times 10^{-9}$ ($R = \sum_i [(\chi_M T)_{\text{obs}} - (\chi_M T)_{\text{calc}}]^2 / \sum_i [(\chi_M T)_{\text{obs}}]^2$). As can be deduced, the two independent sets of values are in good agreement. The ferromagnetic J value can be interpreted as a consequence of the existence of the two azido bridges in *end-on* coordination mode, which gives ferromagnetic coupling. Ruiz et al.^{5a} have shown from density functional theory (DFT) based calculations that there is a correlation between the calculated J parameter and the Cu– N_3 –Cu angle. The theoretical calculation predicted that the J value decreases from a maximum ($J \sim +300$ cm^{-1}) at about $\theta = 90^\circ$ with increasing θ , eventually reaching an antiferromagnetic regime for $\theta > 104\text{--}105^\circ$. The Cu1–N1–Cu1_a angle is found to be 102.4° in 1, which is very common in this kind of complex, and different values of $J > 0$ are reported for the Cu– N_3 –Cu angle.^{5b} In order to clarify our result and compare the J value obtained by the corresponding experimental fits, we have carried out theoretical calculations based on density functional theory (DFT). The J value was obtained via the calculation of the electronic energy of the two different spin configurations ($S = 0$ and $S = 1$ spin states) arising from the coupling between the two unpaired electrons in the dinuclear complex 1 (see ref 16). Such energy calculations were conducted with the Gaussian 09 program,¹⁷ using the B3LYP functional¹⁸ and the TZVP basis set for all atoms.¹⁹ The calculations suggest that $S = 1$ spin state is the stable state and the calculated J value is $+23$ cm^{-1} , which is in good agreement with those obtained from fitting experimental data. The intermolecular antiferromagnetic interactions derive probably from the H-bonding

interaction between the dimers through the perchlorate anions and the NH of the 2-ethylimidazole (Figure S6 in the Supporting Information).

Magnetic Properties of Compound 2. The plot of $\chi_M T$ vs T for compound 2 starts at $0.4 \text{ cm}^3 \text{ mol}^{-1} \text{ K}$ (per one Cu unit) at 300 K (Figure 10a), and with a decrease in temperature there is a monotonic decreasing of $\chi_M T$ until 25 K. Beyond this temperature the $\chi_M T$ value achieves a value close to $0 \text{ cm}^3 \text{ mol}^{-1} \text{ K}$ at 2 K. The $1/\chi_M$ vs T plot shows nonlinearity (Figure S9 in the Supporting Information). The $M/N\beta$ value at 5 T and 2 K reaches a maximum value of $0.34N\beta$ (Figure 10b), which is significantly lower than $2N\beta$ (expected for two unpaired electrons), corroborating the presence of an antiferromagnetic interaction.

To apprehend the type and magnitude of the magnetic exchange interactions, we tried to correlate the data with its structure. Compound 2 is indeed a magnetically 2D system formed by $\mu_{1,3}\text{-N}_3$ bridging of 1D chains where Cu(II) ions are linked together by alternative $\mu_{1,1}\text{-N}_3$ and $\mu\text{-Meimi}^-$ bridging. So far, neither the empirical formula nor computer programs of $\chi_M T$ vs T are available for fitting magnetic data of complicated 2D systems. There are two different Cu– $\mu_{1,3}$ -azido bonds (Cu1–N7 and Cu2–N9) of distances 2.037 and 2.362 Å, respectively. Due to the long distance of the latter one, electron density can be considered as almost zero for the axial position. Thus, for having a rather good approach toward the understanding of exchange interactions, 2 can be considered as a pseudo-1D system, owing to the short intrachain Cu– $\mu_{1,1}$ -azido distances and long intrachain Cu– $\mu_{1,3}$ -azido distances (considering Cu2–N9 bond distance). Indeed, the copper(II) ions are linked by imidazole (antiferromagnetic, AF) and N_3^- (end-on) (ferromagnetic, F), giving an alternating F–AF one-dimensional system.

Borras-Almenar and co-workers reported in 1994 an empirical equation for this kind of Cu(II) alternating chain.¹² In this equation, the parameter α represents the ratio J_F/J_{AF} . Indeed, according to the authors, there are two possibilities for the fit: $0 \leq \alpha \leq 2$ and $2 \leq \alpha \leq 8$. All attempts to fit the data with the latter hypothesis ($2 \leq \alpha \leq 8$) failed. On the contrary, with the first hypothesis, $0 \leq \alpha \leq 2$, we obtained a good fit with the following parameters: $J_{\text{AF}} = -88(2)$ cm^{-1} , $J_F = 101(2)$ cm^{-1} , $g = 2.27(2)$, and $R = 1.2 \times 10^{-4}$. The fitting has been made from 300 to 25 K since the formula employed here¹² is not perfectly valid at very low temperatures. Furthermore, at low temperatures, the interchain $\mu_{1,3}\text{-N}_3$ bridging in 2 would also create a deviation. The values of the fitted parameters agree well with the structural topology of 2. The coupling through

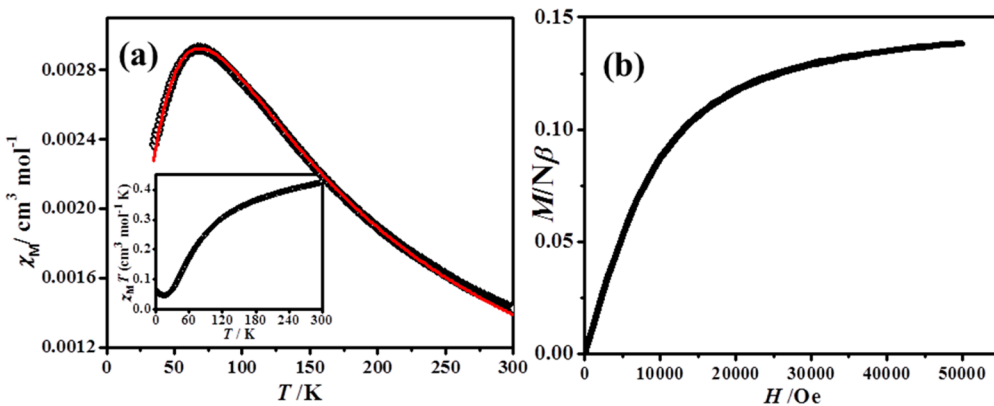


Figure 11. (a) Plot of χ_M vs T for 3 per one Cu center. The solid red line indicates the best fit obtained (see text). Inset shows the plot of $\chi_M T$ vs T for 3 per one Cu center. (b) Plot of the reduced magnetization ($M/N\beta$) (per two Cu centers) at 2 K for compound 3.

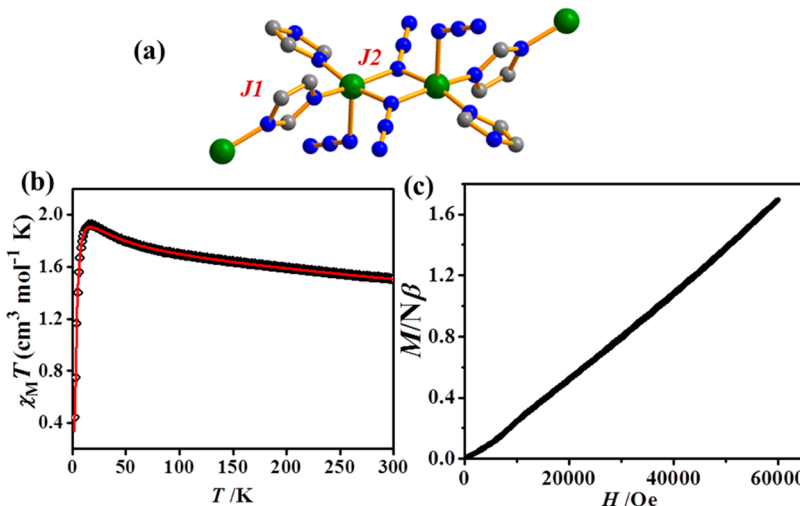


Figure 12. (a) Tetranuclear $[\text{Cu}-(\mu\text{-imi}^{\text{-}})\text{-Cu}-(\mu_{1,1}\text{-N}_3)_2\text{-Cu}-(\mu\text{-imi}^{\text{-}})\text{-Cu}]$ unit considered for modeling the magnetic data. (b) Plot of χ_M vs T for 4 per four Cu centers. The solid red line indicates the best fit obtained (see text). (c) Plot of the reduced magnetization ($M/N\beta$) (per two Cu centers) at 2 K for compound 4.

$\mu_{1,1}\text{-N}_3$ bridging is ferromagnetic as expected,¹³ whereas the 2-methylimidazole bridging ligand creates a strong antiferromagnetic coupling ($J_{\text{AF}} = -88(2)$ cm⁻¹), which agrees well with the literature reports.^{9b,c,14}

Magnetic Properties of Compound 3. For compound 3, the magnetic susceptibility has been measured from 300 to 2 K (Figure 11a) and the magnetization (M vs H) has been measured at 2 K (Figure 11b). At low temperature, the increase in the χ_M value is due to paramagnetic impurities present in the sample. However, the quantity of the impurities must be very small as reflected by the CHN data, and also the powder X-ray diffraction of the sample confirms the phase purity. The $1/\chi_M$ vs T plot shows nonlinearity (Figure S10 in the Supporting Information). Figure 11b shows the plot of the reduced magnetization ($M/N\beta$) (per two Cu centers) at 2 K for compound 3. The $M/N\beta$ value at 5 T and 2 K reaches a maximum value of $0.14N\beta$, which is significantly lower than the expected $2N\beta$ (for ferromagnetically coupled Cu centers), corroborating the presence of an antiferromagnetic interaction.

As revealed by single-crystal X-ray diffraction analysis, compound 3 is two-dimensional. However, it is built from one-dimensional alternating chains (similar to compound 2) linked together by $\mu_{1,3}\text{-N}_3$ ligands. The important structural feature is the coordination of the $\mu_{1,3}\text{-N}_3$ bridge in the axial

position in the square pyramidal geometry of Cu(II) ions (Cu1–N4 and Cu2–N6 bonds). Thus, the unpaired electron is placed in the $x^2 - y^2$ orbital, having an electronic density of almost zero in the apical position (z^2 orbital), and eventually 3 can be considered as a 1D magnetic system. The chain is an alternating antiferromagnetic (imidazole bridge, J_1)–ferromagnetic (end-on azido bridges within the chains, J_2). Hence, the previously mentioned mathematical formula¹² which was used for the analysis of compound 2 can be applied for compound 3, too. However, the mathematical expression is made from the method of closed spin chains of increasing length and is not valid at low temperatures. Furthermore, fitting of the data at low temperature would not be appropriate because of the possible presence of paramagnetic impurities. We have fitted the χ_M vs T data from 300 to 35 K. The presence of a rounded maximum in χ_M close to 75 K is indicative of the antiferromagnetic behavior. In these cases, it is better to fit χ_M than $\chi_M T$. The fit under these conditions is illustrated in Figure 11. The best values obtained are the following: $|J_1| = 63.3(5)$, thus $J_1 = -63.3(5)$ cm⁻¹, $\alpha = 1.5(1)$, giving, thus, $J_2 = 98.1(2)$, and $g = 2.11(1)$, with very good agreement factor, $R = 2.26 \times 10^{-10}$.

The value of the J_1 (antiferromagnetic) must be attributed to the imidazole bridges, which is well reported in the

literature.^{9b,c,14} The ferromagnetic interaction (J_2) originates from two azido ligands in end-on (EO) conformation. According to the reported experimental and theoretical data, this kind of geometry with the corresponding Cu–N_{EO}–Cu angles would give ferromagnetic coupling,^{5b} as it occurs in compound 3.

Magnetic Properties of Compound 4. The plot of $\chi_M T$ vs T for compound 4 is shown in Figure 12 (considering four Cu centers). Starting from 300 K, the $\chi_M T$ values increase up to 16 K, exhibiting a maximum, and then gradually decrease. Above 25 K, the $1/\chi_M$ vs T plot (Figure S11 in the Supporting Information) is well fitted by the Curie–Weiss law ($\chi_M = C/(T - \theta)$), with $C = 1.47 \text{ cm}^3 \text{ mol}^{-1} \text{ K}$ and $\theta = 11.9 \text{ K}$. The positive Weiss constant indicates ferromagnetic interaction operates in 4.

To understand the nature and value of coupling parameters, we have looked at the structure carefully to find an appropriate model to fit the magnetic data. Considering the long interchain Cu– $\mu_{1,3}$ -azido distances, we can safely ignore magnetic interaction between the 1D chains. Now further structural insight into 4 reveals that, in the 1D chains, interaction through the $(\mu_{1,3}\text{-N}_3)_2$ bridging can also be neglected due to the axial coordination of N atom to the Cu(II) center in Cu1–N3 and Cu2–N5 bonds. We have considered a simplified tetranuclear Cu₄ unit [Cu-(μ -imi⁻)–Cu-($\mu_{1,1}\text{-N}_3$)₂–Cu-(μ -imi⁻)–Cu] (Figure 12a) which is linked to the neighboring units by different sets of $\mu_{1,3}$ -azido bridging ligands (where J can be ignored due to long bond distances), giving a 2D network (Figure 7). The fitting has been made assuming the tetranuclear unit with intermolecular interactions ($z'J'$), by means of the MAGPACK program.¹⁵ The best-fit results are the following parameters: J_1 (imidazolate bridge) = $-28.4(2) \text{ cm}^{-1}$; J_2 [$(\mu_{1,1}\text{-N}_3)_2$ bridge] = $16.2(1) \text{ cm}^{-1}$; $g = 2.11(1)$, $z'J' = 1.65(2) \text{ cm}^{-1}$, TIP = $366 \times 10^{-6} \text{ cm}^{-1} \text{ mol}^{-1}$ (TIP, temperature independent paramagnetism), and $R = 2.38 \times 10^{-5}$ (Figure 12). The J values agree with those reported in the literature for similar bridging ligands.^{5b,9c,14} It should be noted that the best fitting gives a small positive $z'J'$ parameter and thus indicates a ferromagnetic intermolecular interaction. This feature is likely due to the fact that these intermolecular interactions are made between magnetic orbitals with the unpaired electron in the z^2 and $x^2 - y^2$ atomic orbitals, respectively (orthogonal to each other).

The $M/N\beta$ value at 6 T and 2 K does not saturate. It reaches a maximum value of $1.7N\beta$ (Figure 12c), which is slightly less than expected: $2N\beta$ (for ferromagnetically coupled two Cu centers). Thus, the dominant interaction between the Cu(II) centers would be ferromagnetic in nature, with a small contribution of an antiferromagnetic interaction, which supports the experimental $\chi_M T$ vs T data and our fitting results.

CONCLUSION

The synthesis, structure, and magnetostructural correlations of metal–azido systems so far reported have mainly focused on longer nonbridging coligands and on several amines. The smaller three-atom bridge imidazolate unit has not been explored properly to date, although it has the potential to fabricate novel magnetic systems. Here we have developed different magnetic systems based on the imidazolate ring along with the azido ligand. We have also shown that structural diversities and versatile magnetic properties could be achieved by changing the substitution on the second linker (imidazole for our work) and employing judicious synthetic strategies. Four Cu(II)-azido coordination compounds with novel

structural motifs and different binding modes of bridging ligands were furnished, and their magnetic studies were studied in detail. Structural insight into these compounds provides explanations for the diverse magnetic behaviors of these compounds. In future, substitution on such imidazole based linkers or other different small organic spacers can be exploited to furnish different metal–azido systems with novel structural topologies and exotic magnetic properties.

ASSOCIATED CONTENT

Supporting Information

Crystallographic data in CIF format. Infrared (IR) spectra, powder X-ray diffraction (PXRD) patterns, reciprocal molar susceptibility vs temperature data, crystal data, and structure refinement parameters for 1–4, 2D H-bonded network of 1, and 2D network of 5. This material is available free of charge via the Internet at <http://pubs.acs.org>.

AUTHOR INFORMATION

Corresponding Author

*E-mail: tmaji@jncasr.ac.in. Tel.: +91 80 2208 2826. Fax: +91 80 2208 2766.

Notes

The authors declare no competing financial interest.

ACKNOWLEDGMENTS

The authors are grateful to the Department of Science and Technology, Government of India, for financial support. The authors are thankful to Prof. A. Sundaresan and Mr. Rana Saha of JNCASR, Bangalore, for magnetic measurements. J.R. acknowledges financial support from the Spanish Government (Grant CTQ2012/30662/BQU).

REFERENCES

- (a) Cheetham, A. K.; Rao, C. N. R. *Science* **2007**, *318*, 58–59.
- (b) Long, J. R.; Yaghi, O. M. *Chem. Soc. Rev.* **2009**, *38*, 1213–1214.
- (c) Yaghi, O. M.; O’Keeffe, M.; Ockwig, N. W.; Chae, H. K.; Eddaoudi, M.; Kim, J. *Nature* **2003**, *423*, 705–714.
- (d) Kurmoo, M. *Chem. Soc. Rev.* **2009**, *38*, 1353–1379.
- (e) Dechambenoit, P.; Long, J. R. *Chem. Soc. Rev.* **2011**, *40*, 3249–3265.
- (f) Rao, C. N. R.; Cheetham, A. K.; Thirumurugan, A. *J. Phys.: Condens. Matter* **2008**, *20*, 083202.
- (g) Mohapatra, S.; Rajeswaran, B.; Chakraborty, A.; Sundaresan, A.; Maji, T. K. *Chem. Mater.* **2013**, *25*, 1673–1679.
- (h) Ribas, J. *Coordination Chemistry*; Wiley-VCH: Weinheim, Germany, 2008; Chapters 5 and 10 and references cited therein.
- (i) Stamatatos, T. C.; Christou, A. G.; Jones, C. M.; O’Callaghan, B. J.; Abboud, K. A.; O’Brien, T. A.; Christou, G. *J. Am. Chem. Soc.* **2007**, *129*, 9840–9841.
- (j) Sarkar, B.; Ray, M. S.; Li, Y.; Song, Y.; Figuerola, A.; Ruiz, E.; Cirera, J.; Cano, J.; Ghosh, A. *Chem.—Eur. J.* **2007**, *13*, 9297–9309.
- (k) Biswas, C.; Drew, M. G. B.; Figuerola, A.; Gómez-Coca, S.; Ruiz, E.; Tangoulis, V.; Ghosh, A. *Inorg. Chim. Acta* **2010**, *363*, 846–854.
- (l) Winpenny, R. E. P. *Angew. Chem., Int. Ed.* **2008**, *47*, 7992–7994.
- (m) Kahn, O. *Molecular Magnetism*; VCH: New York, 1993.
- (n) Chakraborty, A.; Gurunatha, K. L.; Muthulakshmi, A.; Dutta, S.; Pati, S. K.; Maji, T. K. *Dalton Trans.* **2012**, *41*, 5879–5888.
- (o) Chakraborty, A.; Ghosh, B. K.; Arino, J. R.; Ribas, J.; Maji, T. K. *Inorg. Chem.* **2012**, *51*, 6440–6442.
- (p) Chakraborty, A.; Rao, L. S.; Manna, A. K.; Pati, S. K.; Ribas, J.; Maji, T. K. *Dalton Trans.* **2013**, *42*, 10707–10714.
- (q) Chakraborty, A.; Haldar, H.; Maji, T. K. *Cryst. Growth Des.* **2013**, *13*, 4968–4976.
- (r) Ruiz, J.; Mota, A. J.; Diéguez, A. R.; Titos, S.; Herrera, J. M.; Ruiz, E.; Cremades, E.; Costes, J. P.; Colacio, E. *Chem. Commun.* **2012**, *48*, 7916–7918.
- (s) Costes, J. P.; Vendier, L. *Eur. J. Inorg. Chem.* **2010**, *2010* (18), 2768–2773.
- (t) Yuste, C.; Canadilis-Delgado, L.; Labrador, A.; Delgado, F.; Ruiz,

- Perez, C.; Lloret, F.; Julve, M. *Inorg. Chem.* **2009**, *48*, 6630–6640. (m) Fabelo, O.; Pasan, J.; Lloret, F.; Julve, M. *Inorg. Chem.* **2008**, *47*, 3568–3576. (n) Esteban, J.; Font-Bardia, M.; Costa, J. S.; Teat, S. J.; Escuer, A. *Inorg. Chem.* **2014**, *53*, 3194–3203. (o) Alcazar, L.; Cordero, B.; Esteban, J.; Tangoulis, V.; Font-Bardia, M.; Calvet, T.; Escuer, A. *Dalton Trans.* **2013**, *42*, 12334–12345.
- (4) (a) Hay, P. J.; Thibeault, J. C.; Hoffmann, R. J. *J. Am. Chem. Soc.* **1975**, *97*, 4884–4899. (b) Crawford, V. H.; Richardson, H. W.; Wasson, J. R.; Hodgson, D. J.; Hatfield, W. E. *Inorg. Chem.* **1976**, *15*, 2107–2110.
- (5) (a) Ruiz, E.; Cano, J.; Alvarez, S.; Alemany, P. *J. Am. Chem. Soc.* **1998**, *120*, 11122–11129 and references therein. (b) Triki, S.; Gómez-García, C. J.; Ruiz, E.; Sala-Pala, J. *Inorg. Chem.* **2005**, *44*, 5501–5508.
- (6) (a) Song, Y.; Ohkoshi, S.; Arimoto, Y.; Seino, H.; Mizobe, Y.; Hashimoto, K. *Inorg. Chem.* **2003**, *42*, 1848–1856. (b) Mukherjee, P. S.; Maji, T. K.; Mostafa, G.; Mallah, T.; Chaudhuri, N. R. *Inorg. Chem.* **2000**, *39*, 5147–5150. (c) Maji, T. K.; Mukherjee, P. S.; Mostafa, G.; Mallah, T.; Cano-Boquera, J.; Chaudhuri, N. R. *Chem. Commun.* **2001**, 1012–1013. (d) Mondal, K. C.; Mukherjee, P. S. *Inorg. Chem.* **2008**, *47*, 4215–4225. (e) Mukherjee, S.; Gole, B.; Chakrabarty, R.; Mukherjee, P. S. *Inorg. Chem.* **2009**, *48*, 11325–11334. (f) Mukherjee, S.; Gole, B.; Song, Y.; Mukherjee, P. S. *Inorg. Chem.* **2011**, *50*, 3621–3631.
- (7) (a) Wen, H.; Zuo, J.; Liu, W.; Song, Y.; You, X. *Inorg. Chim. Acta* **2005**, 2565–2570. (b) Abu-Youssef, M. A. M.; Escuer, A.; Mautner, F. A.; Ohrstrom, L. *Dalton Trans.* **2008**, 3553–3558. (c) Monfort, M.; Resino, L.; Ribas, J.; Stoeckli-Evans, H. *Angew. Chem., Int. Ed.* **2000**, *39*, 191–193. (d) Gao, E.-Q.; Yue, Y.-F.; Bai, S.-Q.; He, Z.; Yan, C.-H. *J. Am. Chem. Soc.* **2004**, *126*, 1419–1429. (e) Zeng, Y.-F.; Hu, X.; Liu, F.-C.; Bu, X.-H. *Chem. Soc. Rev.* **2009**, *38*, 469–480. (f) Liu, F.-C.; Zeng, Y.-F.; Zhao, J.-P.; Hu, B.-W.; Bu, X.-H.; Ribas, J.; Cano, J. *Inorg. Chem.* **2007**, *46*, 1520–1522.
- (8) (a) Abu-Youssef, A. M.; Escuer, A.; Mautner, F. A.; Öhrström, L. *Dalton Trans.* **2008**, 3553–3558. (b) Liu, F.-C.; Zeng, Y.-F.; Li, J. R.; Bu, X.-H.; Zhang, H. J.; Ribas, J. *Inorg. Chem.* **2005**, *44*, 7298–7300. (c) Liu, F.-C.; Zeng, Y.-F.; Jiao, J.; Li, J. R.; Bu, X.-H.; Ribas, J.; Batten, S. R. *Inorg. Chem.* **2006**, *45*, 6129–6131. (d) Bhowmick, P.; Biswas, S.; Chattopadhyay, S.; Diaz, C.; Gomez-Garcia, C. J.; Ghosh, A. *Dalton Trans.* **2014**, *43*, 12414–12421. (e) Naiya, S.; Biswas, C.; Drew, M. G. B.; Gomez-Garcia, C. J.; Clemente-Juan, J. M.; Ghosh, A. *Inorg. Chem.* **2010**, *49*, 6616–6627. (f) Ray, M. S.; Ghosh, A.; Chaudhuri, S.; Drew, M. G.; Ribas, J. *Eur. J. Inorg. Chem.* **2004**, *2004*, 3110–3117. (g) Colacio, E.; Costes, J.-P.; Domínguez-Vera, J. M.; Maimoun, I. B.; Suárez-Varela, J. *Chem. Commun.* **2005**, 534–536. (h) Thompson, L. K.; Tandon, S. S.; Lloret, F.; Cano, J.; Julve, M. *Inorg. Chem.* **1997**, *36*, 3301–3306. (i) Munno, G. D.; Julve, M.; Viau, G.; Lloret, F.; Faus, J.; Viterbo, D. *Angew. Chem., Int. Ed.* **1996**, *35*, 1807–1810.
- (9) (a) Stamatatos, T. C.; Perlepes, S. P.; Raptopoulou, C. P.; Terzis, A.; Patrickios, C. S.; Tasiopoulos, A. J.; Boudalis, A. K. *Dalton Trans.* **2009**, 3354–3362. (b) Mukherjee, S.; Weyhermüller, T.; Bill, E.; Chaudhuri, P. *Eur. J. Inorg. Chem.* **2004**, *2004*, 4209–4215. (c) Colacio, E.; Domínguez-Vera, J. M.; Ghazi, M.; Kivekas, R.; Klinga, M.; Moreno, J. M. *Inorg. Chem.* **1998**, *37*, 3040–3045. (d) Sakai, K.; Akutagawa, T.; Nakamura, T. *Eur. J. Inorg. Chem.* **2011**, *2011* (1), 116–120. (e) Wu, B.; Wang, S.; Yang, L.; Zhang, T.; Zhang, J.; Zhou, Z.; Yu, K. *Eur. J. Inorg. Chem.* **2011**, *2011* (16), 2616–2623.
- (10) (a) SMART, version 5.628; SAINT, version 6.45a; XPREP, SHELLXTL; Bruker AXS Inc.: Madison, WI, USA, 2004. (b) Sheldrick, G. M. *Siemens Area Detector Absorption Correction Program*; University of Göttingen: Göttingen, Germany, 1994. (c) Altomare, A.; Cascarano, G.; Giacovazzo, C.; Guagliardi, A. *J. Appl. Crystallogr.* **1993**, *26*, 343–350. (d) Sheldrick, G. M. *SHELXL-97, Program for Crystal Structure Solution and Refinement*; University of Göttingen: Göttingen, Germany, 1997. (e) Spek, A. L. *J. Appl. Crystallogr.* **2003**, *36*, 7–13. (f) Farrugia, L. J. *J. Appl. Crystallogr.* **1999**, *32*, 837–838.
- (11) Addison, A. W.; Rao, T. N.; Reedijk, J.; Rijn, J.; Verschoor, G. C. *J. Chem. Soc., Dalton Trans.* **1984**, 1349–1356.
- (12) Borras-Almenar, J. J.; Coronado, E.; Curely, J.; Georges, R.; Gianduzzo, J. C. *Inorg. Chem.* **1994**, *33*, 5171–5175.
- (13) de Biani, F. F.; Ruiz, E.; Cano, J.; Novoa, J. J.; Alvarez, S. *Inorg. Chem.* **2000**, *39*, 3221–3229.
- (14) Koyama, N.; Watanabe, R.; Ishida, T.; Nogami, T.; Kogane, T. *Polyhedron* **2009**, *28*, 2001–2009 and references therein..
- (15) MAGPACK (Magnetic Properties Analysis Package for Spin Clusters)^{15a} employed with a nonlinear least-squares curve-fitting program, DSTEPIT.^{15b} (a) Borrás-Almenar, J. J.; Clemente-Juan, J. M.; Coronado, E.; Tsukerblat, B. S. *J. Comput. Chem.* **2001**, *22*, 985–991; *Inorg. Chem.* **1999**, *38*, 6081–6088. (b) *Program 66*; Quantum Chemistry Program Exchange; Indiana University: Bloomington, IN, USA, 1965.
- (16) Ruiz, E.; Rodríguez-Fortea, A.; Cano, J.; Alvarez, S.; Alemany, P. *J. Comput. Chem.* **2003**, *24*, 982–989.
- (17) Frisch, M. J.; et al. *Gaussian 09*, revision D.01; Gaussian, Inc., Wallingford, CT, USA, 2009.
- (18) Becke, A. D. *J. Chem. Phys.* **1993**, *98*, 5648–5652.
- (19) Schafer, A.; Huber, C.; Ahlrichs, R. *J. Chem. Phys.* **1994**, *100*, 5829–5835.